RSC Advances

PAPER

View Article Online
View Journal | View Issue

Cite this: *RSC Adv.*, 2016, **6**, 31790

Structural diversity in metal–organic nanoparticles based on iron isopropoxide treated lignin†

Kalle Lintinen,[a] Mika Latikka,[b] Mika Henrikki Sipponen,[c] Robin H. A. Ras,[b] Monika Österberg[d] and Mauri A. Kostiainen*[a]

The magnetic nature of iron-containing nanoparticles enables multiple high-end applications. Metal alkoxides are a highly reactive chemical species, which are widely used in ceramics and sol–gel manufacture. However, their use with organic molecules has been mostly limited to catalytic purposes due to their highly reactive nature. Lignin is the second most abundant biopolymer in the world-rich in OH groups and amenable to highly stable colloid nanoparticle formation by a simple solvent exchange process. Here we show that the reaction between iron isopropoxide and lignin in tetrahydrofuran (THF) solution produces metal–organic nanoparticles with tunable morphologies, ranging from hollow and solid nanospheres to open network structures. The immediate condensation reaction between lignin and iron isopropoxide as well as the resulting structure morphology can be controlled by varying the reaction parameters. Despite iron isopropoxide being highly water sensitive, the formed structures are stable as water suspensions. Our results demonstrate that solution processable metal–organic nanoparticles can be easily produced with macromolecular polyols in an inert solvent, such as THF. This presents a facile method of obtaining various metal–organic nanomaterials, with a wide range of metal alkoxides and organic polyols to choose from. We anticipate that metal–bioorganic sol–gel reactions will produce biocompatible materials with enhanced functionality, such as magnetic, antibacterial and catalytic properties depending on the chosen metal and polyol.

Received 11th February 2016
Accepted 21st March 2016

DOI: 10.1039/c6ra03865d

www.rsc.org/advances

1. Introduction

Lignin is the most abundant aromatic polymer on earth. It has thus far been mostly used as a combustion fuel in pulp mills, where the lignin-rich black liquor residue from chemical digestion of wood is combusted to produce energy. Only very recently high-end applications of lignin have started to emerge.[1–3] With the recent advances in black liquor precipitation in the kraft pulping process, lignin is now commercially available on a large scale.[4] Biosynthesized from 4-hydroxyphenylpropanoids or so-called monolignols, lignin is a heterogeneous polymer comprising methoxyl groups as well as phenolic and aliphatic OH functionalities (Fig. S1†). The molecular weight and polydispersity of technical lignin is highly dependent on the source of biomaterial and the isolation process, as the composition varies among plant species and due to the chemical fragmentation of lignin into smaller constituent fractions.[5] Recent studies by Qian *et al.*[6] and Lievonen *et al.*[7] have shown that lignin can be easily formed into relatively monodisperse nanoparticles with excellent colloidal stability. When infused with metal, lignin nanoparticles can retain the functionality of the metal with improved stability and reduced environmental impact.[2]

Metal alkoxides are widely used in the manufacture of ceramics and as catalysts. They have also been used in a number of applications, including for example atomic layer deposition,[8] synthesis of macroporous minerals,[9] catalysts in reaction where CO_2 is a reagent[10] and thin film transistors.[11] Due to the highly reactive nature of metal alkoxides, their use with organic molecules has been limited to catalytic applications, such as polylactide synthesis,[12] vacuum reactions[13] and post-functionalization of preformed metal organic frameworks (MOFs).[14–16] Polyol chelated metals are also widely used in the synthesis of superparamagnetic iron oxide nanoparticles (SPIONs).[17,18] In this polyol process, the polyol chelate is decomposed at high heat to form pure iron oxide.

The standard polyol process can be extended to form metal–organic nanoparticles without the removal of the polyol. If a metal alkoxide is used to bind several polyols together, it can function as molecular 'glue'.[19] With this method it is possible to incorporate metals into an organic matrix, combining the best

[a]*Biohybrid Materials, Department of Biotechnology and Chemical Technology, Aalto University, 00076 Aalto, Finland. E-mail: mauri.kostiainen@aalto.fi*
[b]*Molecular Materials, Department of Applied Physics, Aalto University, 00076 Aalto, Finland*
[c]*Department of Biotechnology and Chemical Technology, Aalto University, 00076 Aalto, Finland*
[d]*Department of Forest Products Technology, Aalto University, 00076 Aalto, Finland*

† Electronic supplementary information (ESI) available. See DOI: 10.1039/c6ra03865d

This journal is © The Royal Society of Chemistry 2016

properties of the organic matrix and the incorporated metal, with possible added functionalities.[20] In the case of colloidal lignin nanoparticles it would be possible to obtain magnetic, non-toxic and colloidally stable metal–organic particles. In the particular case of magnetic resonance imaging (MRI) contrast enhancement, the colloidal stability and possible reduced adverse side effects would offer significant improvement to current commercial SPIONs.[21,22] The embedding of metals into a non-toxic and stable organic framework mimics the way how nature encapsulates reactive metals by using protein cages[23–25] and offers an attractive alternative to the surface modification of iron oxide nanoparticles.[26,27]

We expected lignin either to undergo a chain collapse reaction[28] when used with metal alkoxides, or to be covered with metal oxide layer when used with a lower proportion of lignin. We chose the reaction of iron(III) isopropoxide $Fe(OiPr)_3$ and lignin as a model reaction. The oxides of Fe(III) can either be antiferromagnetic (hematite), ferromagnetic (maghemite) or superparamagnetic (maghemite nanoparticles). The magnetism of soft-matter nanoparticles with bound Fe(III) has not been actively studied recently. Superparamagnetism has been observed in polyvinyl alcohol (PVA) complexed ferritin protein cages, where ferritin has a 12 nm, protein (organic) shell and an iron(III) core.[29]

We also used iron(II) isopropoxide for the reaction with lignin. There are no stable nanoparticles of pure iron(II) oxide, as it tends to disproportionate to Fe and Fe_3O_4. However nanoparticles of iron(II,III) oxide are always (nearly) superparamagnetic and mixed Fe(III) and Fe(II) metal organic frameworks have been shown to be paramagnetic.[30] Thus it was assumed that iron(II) isopropoxide would produce a higher mass magnetization than iron(III) isopropoxide.

When forming metal–organic superstructures with a reaction that is almost immediate upon the contact of the two chemical species, the control of the reaction is extremely challenging and at the same time crucial to the yield of the end product. Here we present a variety of controlled morphologies that were obtained by varying reaction parameters, such as molecular ratio, concentration and temperature. Furthermore, we also show that Fe(II) : lignin nanoparticles have a significantly higher magnetization than Fe(III) : lignin nanoparticles.

2. Experimental section

2.1 Materials

LignoBoost™ softwood kraft lignin was obtained from Stora Enso (Finland). A detailed analysis of the used LignoBoost™ lignin is presented elsewhere.[7] All other chemicals were purchased from Sigma-Aldrich, VWR and Alfa Aesar and were used without further purification.

2.2 $Fe(OiPr)_3$ solution preparation

Sodium (solid block in mineral oil) was reacted with anhydrous 2-propanol under nitrogen atmosphere at 70 °C for 1 h, letting the formed H_2 gas escape (**Warning!**: H_2 is highly flammable when mixed with oxygen, proper ventilation is required), until all of the sodium had reacted into sodium isopropoxide (NaOiPr). $FeCl_3$ was dissolved in anhydrous 2-propanol and the solution was added to the 2-propanol solution of NaOiPr. The solution gradually turned dark brown, after which the solution was cooled to room temperature and the formed NaCl (pale yellow due to traces of iron) was precipitated and removed by centrifugation. The black $Fe(OiPr)_3$ 2-propanol solution was used as such or with further dilution in anhydrous THF.

2.3 $Fe(OiPr)_2$ solution preparation

The solution was prepared exactly as the $Fe(OiPr)_3$, but with anhydrous $FeCl_2$.

2.4 Lignin solution preparation

LignoBoost™ lignin was dissolved in anhydrous THF with molecular sieves (0.3 nm) added to capture any residual water from the already dried lignin.

2.5 Condensation reactions

The general method of reaction was the addition of a THF solution of $Fe(OiPr)_3$ or $Fe(OiPr)_2$ or a 2 : 1 mixture of both into a THF solution of lignin, resulting in an immediate condensation.

2.6 Hydrolysis reactions

The general method of hydrolysis was the addition of an equal volume of 1 wt% water in THF into a solution of Fe : lignin in THF. After the particles were hydrolyzed, they were solvent exchanged in a dialysis tube (12–14 kDa cut off) immersed in deionized water, with the dialysis water changed at least once to minimize the residual solvent (THF and isopropanol) in the dispersion. Further purification was not required as the only byproduct of the reaction was the released isopropanol.

Full experimental details for the preparation of Samples 1–4 are presented in the ESI.†

2.7 Characterization techniques

Transmission electron microscopy (TEM) was performed on a FEI Tecnai 12 operating at 120 kV and FEI Tecnai 20 operating at 200 kV. Particle dispersions were dried on carbon film support grid. Imaging was carried out in bright-field mode with slight underfocus. AAS was measured with Varian 240 Atomic Absorption Spectrometer, using air–acetylene flame. The radiation source was a hollow cathode lamp and the measurement wavelength was 248.3 nm. DLS and ζ-potential analyses were carried out with a Zetasizer Nano S from Malvern Instruments at 25 °C. Results were the average of at least five measurements. The infrared spectra were recorded using an FTIR-ATR-MATTSON 3000-FTIR spectrometer. ^1H and ^{31}P NMR spectra were measured from the lignin materials. The ^{31}P NMR procedure involved dissolution of 30 mg of lignin in a mixture of dimethylformamide (0.15 mL) and pyridine (0.10 mL), followed by the addition of 0.20 mL of *endo-N*-hydroxy-5-norbornene-2,3-dicarboximide (9.37 mg mL^{-1}) in pyridine : deuterated chloroform solvent mixture (1.6 : 1, v/v). Chromium(III) acetylacetonate (0.05 mL, 0.58 mg in the above solvent mixture) was added

as a relaxation agent. 2-Chloro-4,4,5,5-tetramethyl-1,3,2-dioxaphospholane (0.15 mL) was added slowly to start the phosphitylation reaction. Finally, 0.3 mL of deuterated chloroform was added, and the clear solution was analyzed with a Bruker Avance III 400 MHz spectrometer, recording 512 scans at 30° pulse angle, 5 s relaxation time and 1.1 s acquisition time. Peaks were assigned according to the standard method.[31] The magnetic properties of the lignin nanoparticles were measured with a vibrating sample magnetometer (VSM, Quantum Design PPMS Dynacool). Measurements were performed with standard polypropylene powder cups with approximately 5–7 mg of sample powder (nanoparticles) or dispersion (open network structure). Liquid samples were sealed with vacuum grease and parafilm. Hysteresis loops were measured with 1 mm peak amplitude and 40 Hz frequency between −9 and 9 T in 300 K. Background from the sample holder was subtracted from results by performing similar blank measurements for water-filled powder cup as well as empty powder cup with vacuum grease and parafilm.

3. Results and discussion

3.1 Preparation and imaging of Fe : lignin nanoparticles

Both $Fe(OiPr)_3$ and lignin are readily soluble in THF and are stable as anhydrous solutions. The colors of both solutions range from yellow to black, depending on their concentration (Fig. S5†). All condensation reactions described in this section were conducted in anhydrous THF. Fig. 1 shows an idealized representation of the lignin–iron condensation reaction and describes the hydrolysis step. Firstly $Fe(OiPr)_3$ solution is added into lignin solution, resulting in the condensation of the accessible OH groups, releasing isopropanol and forming Fe–O–C_{lignin} bonds. Secondly the Fe(OiPr) moieties on the surface of the formed composite are hydrolyzed to finalize the reaction, releasing isopropanol (formation of Fe–O–Fe bonds). In practice the condensation reaction 1° takes place between several lignin and $Fe(OiPr)_3$ molecules, creating amorphous lignin clusters. The hydrolysis reaction 2° can take place within just one Fe(OiPr) coated cluster, or the hydrolysis can fuse several clusters together. Adding an excess of water also collapses the hydrophobic lignin into roughly spherical clusters.

When a $Fe(OiPr)_3$ solution was added to a lignin solution at room temperature and at relatively high concentration, in 1 : 1 OH_{lignin} : $Fe(OiPr)_3$ ratio, a black precipitate formed immediately and the solution become otherwise transparent, indicating a full consumption of both reagents. The precipitate could be redispersed by diluting with THF and sonication. When the condensate was hydrolyzed with the addition of 10 wt% of deionized water in THF, a fishnet-type open network structure with particle sizes from below 100 nm to several μm was observed (Fig. 2: Sample 1). This structure can be explained by the immediate condensation reaction occurring as 10 to 30 nm iron–lignin nanoparticles fuse together with Fe–O–Fe bonds. The open network structure, formed with the uncontrolled hydrolysis, cannot be converted into uniform spheres. It is possible to further react the unhydrolyzed particles with lignin to form solid particles that are highly non-uniform and rough in shape (Fig. S3†).

With 1 : 1 OH : $Fe(OiPr)_3$ ratio, the formation of uniform spherical nanoparticles requires both the condensation and hydrolysis steps to be conducted in dilute solutions and the condensation step to be conducted at a reduced temperature. With 2.1 mg g^{-1} of lignin and 0.9 mg g^{-1} of $Fe(OiPr)_3$ in THF, and the condensation conducted in acetone ice (*ca.* −95 °C), a clear orange solution was obtained. Spherical particles with the diameter of 10 to 30 nm were formed exclusively when the hydrolysis was conducted at room temperature with the dropwise addition of 1 wt% deionized water in THF (Fig. 2: Sample 2).

An exact equimolar ratio of lignin OH to $Fe(OiPr)_3$ would translate to *ca.* 1 nm nanoparticles (a single lignin molecule with an average mass of *ca.* 5 kDa [see ESI†], covered with Fe_2O_3), which we have not observed. Instead several lignin

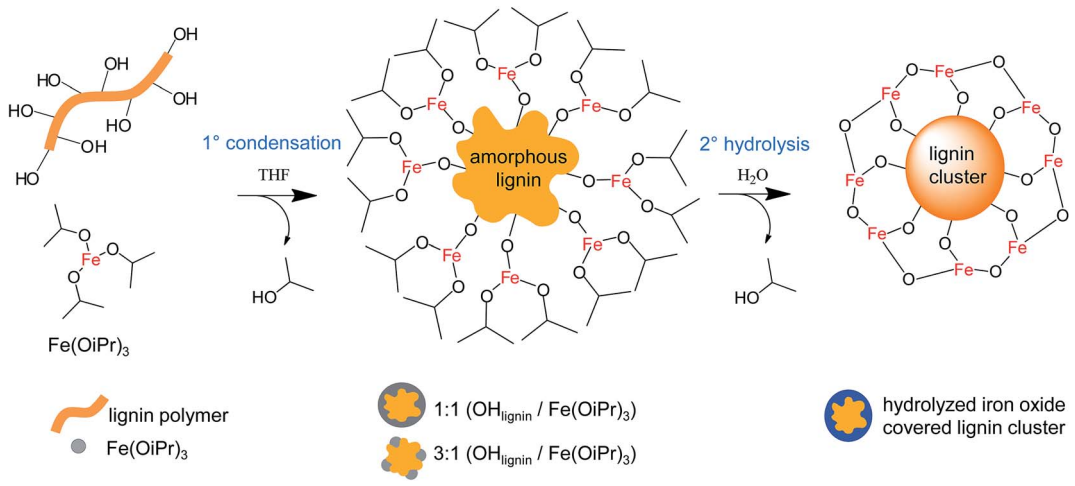

Fig. 1 Idealized reaction scheme between lignin and $Fe(OiPr)_3$: (1°) all of the accessible OH groups of lignin condense with $Fe(OiPr)_3$, releasing isopropanol and forming amorphous lignin clusters. The coverage of Fe(OiPr) moieties on lignin can be tuned by adjusting the OH_{lignin} : $Fe(OiPr)_3$ ratio. (2°) The hydrolysis of the isopropoxy groups results in the condensation of adjacent Fe(OiPr) moieties.

This journal is © The Royal Society of Chemistry 2016

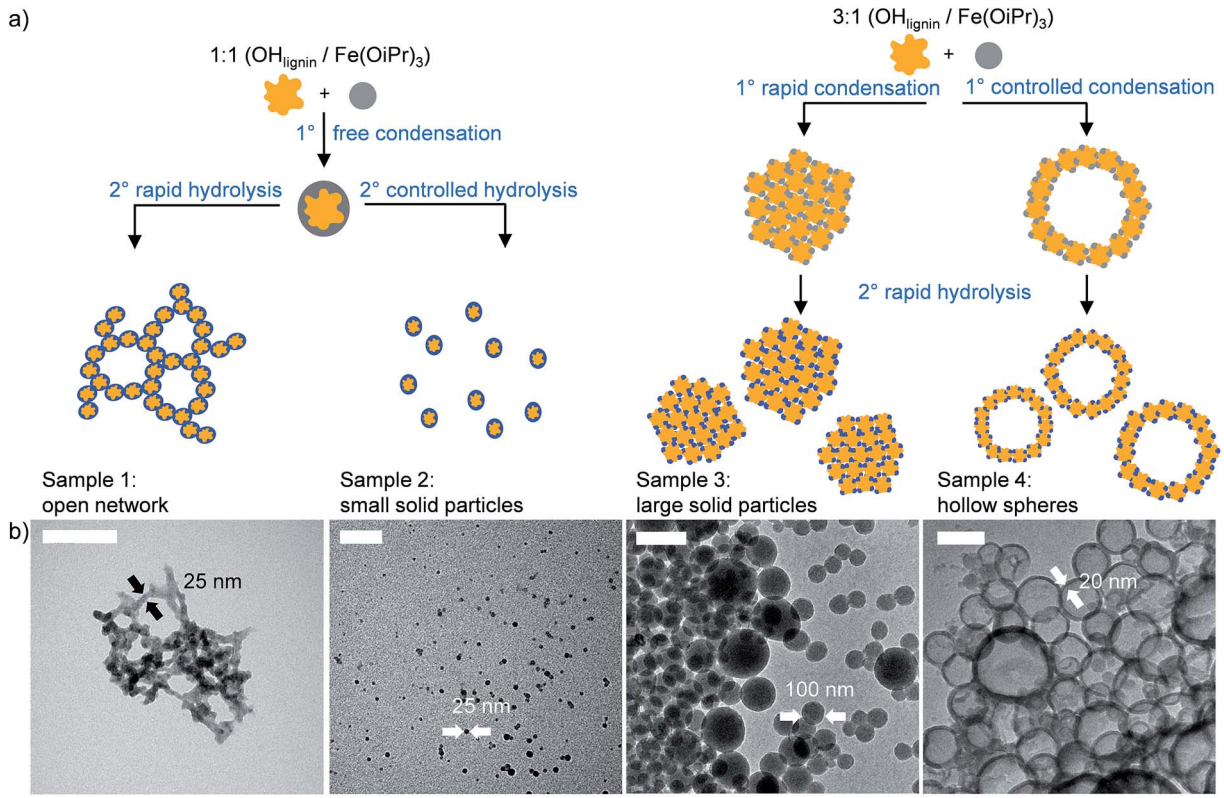

Fig. 2 Different nanoparticle morphologies achieved by varying the reaction parameters. (a) Schematic presentation and (b) TEM images of the obtained structures. Sample 1: rapid hydrolysis fuses Fe(OiPr) coated Fe : lignin nanoparticles into fishnet-type open network structures. Sample 2: controlled hydrolysis keeps the Fe : lignin nanoparticles from fusing together and yields small solid particles. Sample 3: when less Fe(OiPr)$_3$ is used than the accessible OH groups in lignin, the lignin clusters are partially covered with Fe(OiPr) moieties. The partially covered clusters fuse together to form larger (*ca.* 200 nm) particles. Sample 4: when less Fe(OiPr)$_3$ is used than the accessible OH groups and the solutions are slow, the fusing of Fe : lignin nanoparticles create hollow spheres. Scale bars in all TEM images are 200 nm.

chains are bound together during the initial condensation step. However the equimolar ratio of OH to Fe(OiPr)$_3$ can be considered an upper limit for Fe(OiPr)$_3$, above which the unreacted Fe(OiPr)$_3$ will react with itself and form oxidized iron particles upon hydrolysis. Fig. 1 has to be considered a simplification of the condensation reaction between the non-spherical lignin and Fe(OiPr)$_3$ molecules, especially with high Fe(OiPr)$_3$ ratios. When the ratio of OH groups was increased to 3 : 1 OH$_{lignin}$: Fe(OiPr)$_3$, a full condensation of OH groups with Fe(OiPr) moieties can be obtained to yield much larger structures. With 3 : 1 OH$_{lignin}$ to Fe(OiPr)$_3$ ratio, the reaction is also much more robust, as the larger nanoparticles form before hydrolysis. Concentrations at least up to 20 mg g^{-1} of lignin and 30 mg g^{-1} of Fe(OiPr)$_3$ can be condensed at room temperature to produce relatively monodisperse particles, mostly between 50 and 400 nm (Fig. 2: Sample 3).

Theoretically an even lower concentration of Fe(OiPr)$_3$ to lignin OH groups could be considered, but practically this can easily lead to a mixture of condensed (3 : 1 OH$_{lignin}$: Fe(OiPr)$_3$ ratio) nanoparticles and iron free lignin. The residual unreacted lignin can be collapsed into colloidal nanoparticles through the gradual increase of polarity with the addition of water.[7] The dependence of the formed structure on the lignin OH to Fe(OiPr)$_3$ ratio is depicted in closer detail in the ESI (Fig. S4†).

When lignin and Fe(OiPr)$_3$ solutions are separated by a 3 μm pore size polytetrafluoroethylene (PTFE) membrane and allowed to mix through it at room temperature, an exclusive formation of hollow spheres can be achieved (3 : 1 ratio of lignin OH groups to Fe(OiPr)$_3$). This can be explained by the condensation reaction occurring at the membrane as soon as the two solutions diffuse into each other. The reaction at room temperature is fast enough so that the forming complex cannot collapse into a solid sphere. The most probable location where

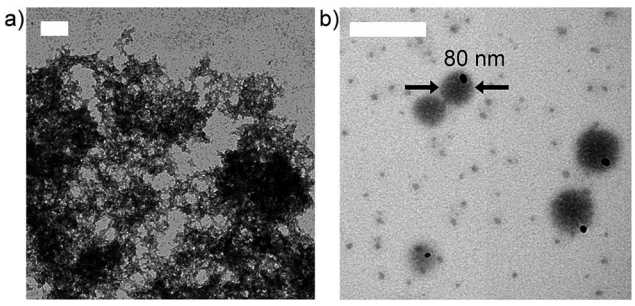

Fig. 3 (a) Formation of a macroscopic network upon the addition of lignin into Fe(OiPr)$_3$ (reverse order). (b) Separation of Fe_2O_3 nanoparticles from Fe : lignin assemblies upon heating to 95 °C. Scale bar 200 nm.

the $Fe(OiPr)_3$ molecule will react with the growing Fe–O–lignin polymer is at the edges of the condensate, consequently favoring the formation of large hollow spheres with a diameter of 100–400 nm (Fig. 2: Sample 4).

A notable point in the reaction between lignin and $Fe(OiPr)_3$ is that the condensation reaction takes place immediately upon contact of the lignin OH and the iron isopropoxy groups. When lignin solution is added into an $Fe(OiPr)_3$ solution (reverse order), a large unstructured macroscopic network is formed (Fig. 3a). It can be assumed that applications could be found for this kind of additive assembly polymer formation, such as an inexpensive alternative to porous metal–organic frameworks (MOFs).

The assumption of the iron–lignin composite structure was that the particles are assemblies with C_{lignin}–O–Fe–O–C_{lignin} bonds, rather than the particles being composed of separate lignin and Fe_2O_3 domains. While infrared (IR) spectra and atomic absorption spectroscopy (AAS) measurements support the hypothesis, a visual indication for this is observed from an experiment where a nanoparticle sample was dried at 95 °C and rehydrated in deionized water. The TEM image of the particles showed lighter colored spheres, which had ~15 nm dark spots within them (Fig. 3b), indicating a separation of iron into a Fe_2O_3 nanoparticle (possible temperature induced oxidation with ambient oxygen). This phenomenon could be used to increase the mass magnetization of the Fe : lignin particles.

3.2 Chemical composition of Fe : lignin particles

The iron content of the particles was measured by AAS. When the reaction was conducted with an equimolar ratio of OH groups to $Fe(OiPr)_3$ the particles contained 29.7 wt% Fe, which is in good accordance with the condensation/hydrolysis reaction. A more detailed discussion of the iron content analysis is presented in the ESI.† The presence of bound iron can also be observed in the IR spectra of the particles (Fig. 4). The most notable difference between the IR spectra of lignin *versus* the Fe : lignin polymer is the disappearance of the 1700 cm^{-1} carboxyl/carbonyl band. A strong indication of the formation of a Fe–O–Fe oxo complex is the appearance of a clear band at 668 cm^{-1}.[32] The OH stretch at 3440 cm^{-1} for lignin has also shifted to 3349 cm^{-1}. Additional bands at 1648 cm^{-1}, 1379 cm^{-1}, 887 cm^{-1}, 721 cm^{-1}, 616 cm^{-1} and 500 cm^{-1}, correspond well with known iron oxide/organic IR spectra.[33,34] The comparison with Fe_2O_3 flakes prepared by the hydrolysis of $Fe(OiPr)_3$ indicate that the additional bands to lignin are not caused by the superposition of the Fe_2O_3 spectrum onto the lignin spectrum. Rather the results indicate that the bonds formed are Fe–O–C alkoxy bonds, with additional Fe–O–Fe oxo complexes formed upon the hydrolysis of the Fe(OiPr) surface of the Fe : lignin polymer. The comparison of the Fe(III) : lignin and Fe(II) : lignin polymers is presented in the ESI.†

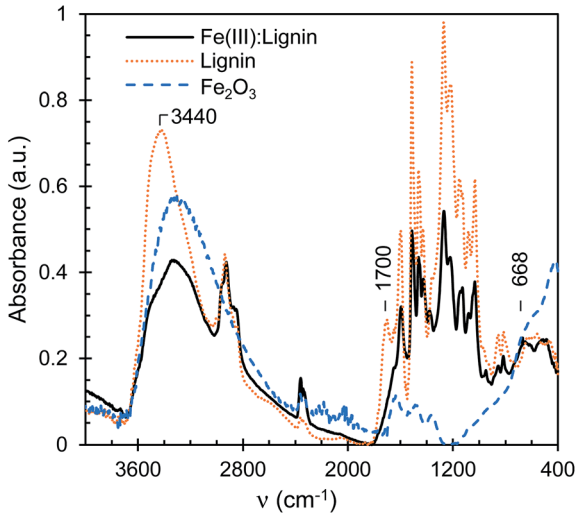

Fig. 4 Normalized IR spectra of pure lignin (orange dotted), Fe(III) : lignin polymer (solid black) and Fe_2O_3 (dashed blue). 3440 cm^{-1} ν(OH); 1700 cm^{-1} ν(C=O); 668 cm^{-1} ν(Fe–O–Fe).

3.3 Colloidal stability of the Fe : lignin complexes

Dynamic light scattering (DLS) was used to confirm the nanoparticle sizes observed by TEM and to determine their polydispersity, while ζ-potential was measured to study the surface charge of the colloids. Fe(III) : lignin nanoparticles prepared with a 3 : 1 OH : $Fe(OiPr)_3$ ratio (Sample 3) had a relatively narrow size distribution (polydispersity index, PDI = 0.150) and intensity–average hydrodynamic diameter D_h = 252 nm, matching well with the TEM data. The measured ζ-potential was −39.8 mV, indicating a negative charge and suggesting that the particles are electrostatically stabilized (Fig. 5). Filtered Fe(III) : lignin nanoparticles prepared with a 1 : 1 OH : $Fe(OiPr)_3$ ratio (Sample 2) had a significantly smaller size (D_h = 125 nm, PDI = 0.182) and a ζ-potential of −24.7 mV. Despite the lower particle size of 1 : 1 OH : $Fe(OiPr)_3$ nanoparticles, the ζ-potential is more negative with 3 : 1 OH : $Fe(OiPr)_3$ nanoparticles, due to the presence of larger amount of free negatively charged lignin.

3.4 Magnetic properties of the Fe : lignin polymers

The assumption was that the Fe(III) : lignin composites would be weakly if at all magnetic. Therefore nanoparticle formation was also conducted with lignin and a 1 : 2 mixture of $Fe(OiPr)_2$ and $Fe(OiPr)_3$ with the purpose to obtain a magnetite [Fe_3O_4] analogue, which should have increased magnetic properties.

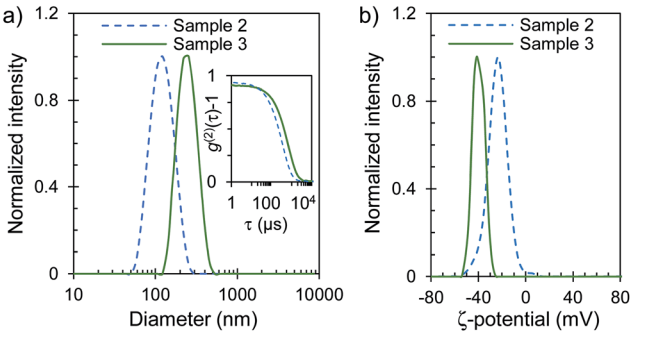

Fig. 5 (a) DLS intensity–average size distributions (inset shows the corresponding second-order correlation curves) and (b) ζ-potential graphs of 1 : 1 OH : $Fe(OiPr)_3$ small solid nanoparticles (Sample 2, blue dashed) and 3 : 1 OH : $Fe(OiPr)_3$ nanoparticles (Sample 3, green solid).

This journal is © The Royal Society of Chemistry 2016

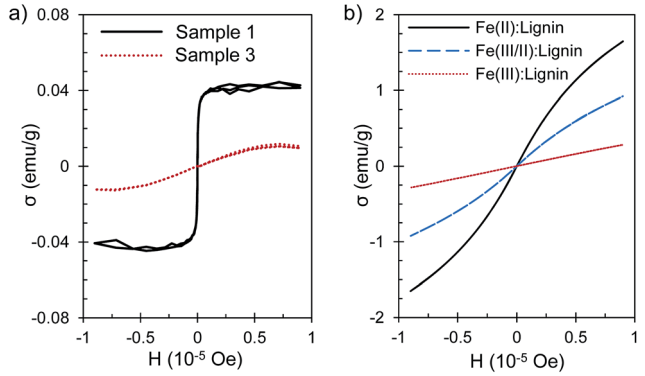

Fig. 6 Mass magnetization of lignin–iron composites. (a) Fe(III) : lignin network structures (Sample 1, solid black) and Fe(III) : lignin large solid nanoparticles (Sample 3, dashed red) with paramagnetic component subtracted. (b) Fe(III) : lignin large solid nanoparticles (Sample 3, dashed red); 2 : 1 Fe(III) : Fe(II) : lignin large solid nanoparticles (dashed blue); Fe(II) : lignin NP (solid black).

Nanoparticles were also prepared from lignin and $Fe(OiPr)_2$, to obtain a wüstite [Fe(II)O] analogue, even though Fe(II) oxide nanoparticles are not generally used due to their propensity to oxidize spontaneously.[27,32,35,36] As the reaction with lignin does not produce iron oxides, spontaneous oxidation or disproportionation was not expected.

The Fe(III) : lignin open network structures (Sample 1) were consistent with superparamagnetic material, with a saturation magnetization of 0.041 emu g^{-1} (Fig. 6). It seems that the size of *ca.* 15 nm of the branches is sufficiently low to allow for superparamagnetism. The magnitude of mass magnetization is rather small compared to pure γ-Fe_2O_3 (maghemite) nanoparticles, which can have magnetization up to *ca.* 100 emu g^{-1}.[37] Even when taking account the lower iron content of the Fe : lignin particles, the mass magnetization is rather low, which can be explained by the fact that the iron atoms are bound to lignin and the quenching effect of the organic matrix can be significant.[38]

The size of the larger (200–400 nm) solid spheres (Sample 3) of Fe(III) : lignin was too large for pure superparamagnetism, but clear paramagnetism was observed, with a mass susceptibility of 2.7×10^{-6} emu g^{-1} Oe^{-1}. In comparison, Fe(III/II) : lignin and Fe(II) : lignin nanoparticles have much higher mass susceptibilities (1.4×10^{-5} emu g^{-1} Oe^{-1} and 3.1×10^{-5} emu g^{-1} Oe^{-1} respectively). The ratio of susceptibilities suggests that the mass susceptibility of Fe(III/II) : lignin is a sum of Fe(II) : lignin and Fe(III) : lignin components (calculated to be 1.2×10^{-5} emu g^{-1} Oe^{-1}) (Fig. 6).

4. Conclusions

We have demonstrated that the extreme reactivity of iron isopropoxide ($Fe(OiPr)_3$) with lignin hydroxyl groups can be harnessed to form a range of metal–organic nanoparticle morphologies. The nanoparticle morphology can be tuned by adjusting the condensation and hydrolysis reaction parameters to yield reproducibly four different states: (1) a fishnet-type open network structure, (2) small solid particles with a diameter of 10–30 nm, (3) large uniform spheres with diameters ranging between 50–400 nm and (4) hollow nanoparticles.

Nanoparticles can also be produced with $Fe(II)(OiPr)_2$ or a with a mixture of $Fe(III)(OiPr)_2$ and $Fe(II)(OiPr)_3$, yielding particles with increased mass magnetization. Furthermore, the magnetic properties are determined by the specific particle size and morphology. The particles with sizes below 50 nm show clear superparamagnetic characteristics, whereas particles of larger sizes also have a paramagnetic component.

Taken together, these observations show that iron isopropoxide functions as a molecular glue that can be controlled to bind the organic polyol lignin into a variety of nanostructure morphologies. We expect that this property can be generalized to many other metal alkoxides and macromolecular polyols. Considering that plant-based macromolecular polyols, such as lignin and cellulose are renewable, readily available, inexpensive and metal alkoxides are easy to produce and relatively inexpensive, the future potential for these types of metal–organic materials is considerable. Depending on the chosen macromolecular polyol and metal alkoxide, the characteristics of such materials can vary from magnetic,[39] antibacterial, catalytic, photonic, mechanical to gas and moisture barrier properties.

Acknowledgements

Financial support from the Aalto University (Forest Meets Chemistry project) Academy of Finland (Grants 263504, 267497, 273645), Biocentrum Helsinki and Emil Aaltonen Foundation is gratefully acknowledged. This work was carried out under the Academy of Finland's Centers of Excellence Programme (2014–2019) and made use of the Aalto University Nanomicroscopy Centre (Aalto NMC).

References

1 A. J. Ragauskas, G. T. Beckham, M. J. Biddy, R. Chandra, F. Chen, M. F. Davis, B. H. Davison, R. A. Dixon, P. Gilna, M. Keller, P. Langan, A. K. Naskar, J. N. Saddler, T. J. Tschaplinski, G. A. Tuskan and C. E. Wyman, *Science*, 2014, **344**, 1246843.
2 A. P. Richter, J. S. Brown, B. Bharti, A. Wang, S. Gangwal, K. Houck, E. A. Cohen Hubal, V. N. Paunov, S. D. Stoyanov and O. D. Velev, *Nat. Nanotechnol.*, 2015, **10**, 817–823.
3 W.-J. Liu, H. Jiang and H.-Q. Yu, *Green Chem.*, 2015, **17**, 4888–4907.
4 P. E. R. Tomani, *Cellul. Chem. Technol.*, 2010, **44**, 53–58.
5 A. Tolbert, H. Akinosho and R. Khunsupat, *Biofuels, Bioprod. Biorefin.*, 2014, **8**, 836–856.
6 Y. Qian, Y. Deng, X. Qiu, H. Li and D. Yang, *Green Chem.*, 2014, 1–10.
7 M. Lievonen, J. J. Valle-Delgado, M.-L. Mattinen, E.-L. Hult, K. Lintinen, M. A. Kostiainen, A. Paananen, G. R. Szilvay, H. Setälä and M. Österberg, *Green Chem.*, 2016, **18**, 1416–1422.
8 M. Ritala, *Science*, 2000, **288**, 319–321.

9 B. T. Holland, *Science*, 1998, **281**, 538–540.
10 Q. Liu, L. Wu, R. Jackstell and M. Beller, *Nat. Commun.*, 2015, **6**, 5933.
11 K. K. Banger, Y. Yamashita, K. Mori, R. L. Peterson, T. Leedham, J. Rickard and H. Sirringhaus, *Nat. Mater.*, 2011, **10**, 45–50.
12 P. Dubois, C. Jacobs, R. Jerome and P. Teyssie, *Macromolecules*, 1991, **24**, 2266–2270.
13 J. T. Korhonen, P. Hiekkataipale, J. Malm, M. Karppinen, O. Ikkala and R. H. A. Ras, *ACS Nano*, 2011, **5**, 1967–1974.
14 K. L. Mulfort, O. K. Farha, C. L. Stern, A. A. Sarjeant and J. T. Hupp, *J. Am. Chem. Soc.*, 2009, **131**, 3866–3868.
15 R. B. Getman, J. H. Miller, K. Wang and R. Q. Snurr, *J. Phys. Chem. C*, 2011, **115**, 2066–2075.
16 K. Suzuki, S. Sato and M. Fujita, *Nat. Chem.*, 2010, **2**, 25–29.
17 P. Toneguzzo, G. Viau, O. Acher, F. Fiévet-Vincent and F. Fiévet, *Adv. Mater.*, 1998, **10**, 1032–1035.
18 D. Caruntu, G. Caruntu, Y. Chen, C. J. O. Connor, G. Goloverda and V. L. Kolesnichenko, *Chem. Mater.*, 2004, **16**, 5527–5534.
19 S. L. Bernasek, J. Schwartz, A. B. Bocarsly, G. Lu, K. Purvis and S. Vanderkam in *Fundamental and Applied Aspects of Chemically Modified Surfaces*, ed. J. P. Blitz and C. B. Little, Woodhead Publishing, 1999, pp. 341–348.
20 Z. Nie, A. Petukhova and E. Kumacheva, *Nat. Nanotechnol.*, 2010, **5**, 15–25.
21 S. Balasubramaniam, S. Kayandan, Y.-N. Lin, D. F. Kelly, M. J. House, R. C. Woodward, T. G. St Pierre, J. S. Riffle and R. M. Davis, *Langmuir*, 2014, **30**, 1580–1587.
22 S. Tähkä, A. Laiho and M. A. Kostiainen, *Chem.–Eur. J.*, 2014, **20**, 2718–2722.
23 N. D. Chasteen and P. M. Harrison, *J. Struct. Biol.*, 1999, **126**, 182–194.
24 M. Uchida, M. T. Klem, M. Allen, P. Suci, M. Flenniken, E. Gillitzer, Z. Varpness, L. O. Liepold, M. Young and T. Douglas, *Adv. Mater.*, 2007, **19**, 1025–1042.
25 M. A. Kostiainen, P. Ceci, M. Fornara, P. Hiekkataipale, O. Kasyutich, R. J. M. Nolte, J. J. L. M. Cornelissen, R. D. Desautels and J. van Lierop, *ACS Nano*, 2011, **5**, 6394–6402.
26 J. J. J. Yang, L. Wei, O. Zurkiya, W. Yang, S. Li, J. Zou, Y. Zhou, A. L. W. Maniccia, H. Mao, F. Zhao, R. Malchow, S. Zhao, J. Johnson, X. Hu, E. Krogstad and Z.-R. Liu, *J. Am. Chem. Soc.*, 2008, **130**, 9260–9267.
27 H. Markides, M. Rotherham and A. J. El Haj, *J. Nanomater.*, 2012, **2012**, 1–11.
28 S. Mavila, C. E. Diesendruck, S. Linde, L. Amir, R. Shikler and N. G. Lemcoff, *Angew. Chem., Int. Ed. Engl.*, 2013, **52**, 5767–5770.
29 J. H. Jung, Y. H. Hyun, S. Y. Park, Y. P. Lee, M. K. Shin and S. J. Kim, *J. Korean Phys. Soc.*, 2011, **58**, 797–800.
30 J.-P. Zhao, B.-W. Hu, F. Lloret, J. Tao, Q. Yang, X.-F. Zhang and X.-H. Bu, *Inorg. Chem.*, 2010, **49**, 10390–10399.
31 M. Balakshin and E. Capanema, *J. Wood Chem. Technol.*, 2015, **35**, 220–237.
32 C. E. MacBeth, A. P. Golombek, V. G. Young, C. Yang, K. Kuczera, M. P. Hendrich and A. S. Borovik, *Science*, 2000, **289**, 938–941.
33 B. M. Conceição, M. A. S. Costa, L. C. D. S. Maria, M. R. Silva and S. H. Wang, *Polimeros*, 2011, **21**, 409–415.
34 J. Cejka, J. Sejkora, J. Plášil, S. Bahfenne, S. J. Palmer and R. L. Frost, *Spectrochim. Acta, Part A*, 2011, **79**, 1356–1363.
35 M. Mozaffari, M. Gheisari, M. Niyaifar and J. Amighian, *J. Magn. Magn. Mater.*, 2009, **321**, 2981–2984.
36 A. Navrotsky, C. Ma, K. Lilova and N. Birkner, *Science*, 2010, **330**, 199–201.
37 M. Mohapatra and S. Anand, *Int. J. Eng. Sci. Tech.*, 2010, **2**, 127–146.
38 M. F. Barnothy, *Biological Effects of Magnetic Fields*, 1995, vol. 2.
39 Z. Song, W. Li, W. Liu, Y. Yang, N. Wang, H. Wang and H. Gao, *RSC Adv.*, 2015, **5**, 13028–13035.

This journal is © The Royal Society of Chemistry 2016